Int. J. Electrochem. Sci., 15 **(2020)** 208 – 222, doi: 10.20964/2020.01.31

International Journal of
ELECTROCHEMICAL
SCIENCE
www.electrochemsci.org

Synergistic Effects of a Sulfate-Reducing Bacteria and an Applied Stress on the Corrosion Behavior of 17-4 PH Stainless Steel After Different Heat Treatments

Ming Wu[1,*], *Zhihao Zhao*[1], *Xu Wang*[2,3,*], *J. C. Huang*[3], *Xinyi Liu*[2]

[1] College of Petroleum Engineering, Liaoning Shihua University, Fushun, Liaoning, 113001, China
[2] School of Mechanical Engineering, Liaoning Shihua University, Fushun, Liaoning 113001, China
[3] Department of Materials Science and Engineering, Hong Kong Institute for Advanced Study, City University of Hong Kong, Kowloon, Hong Kong
[*]E-mail: wuming0413@163.com, wangxu@lnpu.edu.cn

Received: 16 August 2019 / *Accepted:* 18 October 2019 / *Published:* 30 November 2019

The individual and synergistic effects of sulfate-reducing bacteria (SRB) and an applied stress on the corrosion behavior of 17-4 precipitation-hardened (PH) stainless steel in sterile and SRB-inoculated solutions were investigated by electrochemical impedance spectroscopy and fractographic observation. Different heat treatments were applied to the 17-4 PH stainless steel, including single-stage aging, double-stage aging, and an intermediate treatment. The microstructures of the 17-4 PH stainless steels were mainly composed of lath martensite. However, the samples subjected to an intermediate treatment showed improved toughness as a result of the uniform and fine lath martensite. Among the samples considered in this study, the double-stage aged samples exhibited the highest yield strength and maximum stress corrosion cracking (SCC) susceptibility (I_{scc}) of 43.2% in the sterile solution. In the SRB-inoculated solution, the impedance values of all samples were reduced, and the production of harmful metabolites, such as FeS and H_2S, occurred, indicating that SRB promoted corrosion of the stainless steel. The double-stage aged samples were the most sensitive to the SRB among the samples considered herein, where the I_{scc} was 52.8%. The SCC mechanism for single-stage aged and intermediate-treated samples was anodic dissolution (AD), and that for the double-stage aged samples was hydrogen induced cracking (HIC).

Keywords: 17-4 PH stainless steel, applied stress, sulfate-reducing bacteria, stress corrosion cracking

1. INTRODUCTION

Precipitation-hardened (PH) stainless steel, with excellent corrosion resistance and extraordinary mechanical properties, can be obtained by aging treatment of the stainless steel. The excellent corrosion resistance is due to a chromium content of at least 12 wt.% [1]. The extraordinary mechanical properties result from the uniform distribution of alloying elements during precipitation hardening [2, 3]. A typical stainless steel, 17-4 PH stainless steel, has been widely used in drilling platforms and offshore pipelines [4, 5]. It is susceptible to stress corrosion cracking (SCC) due to the combined effects of stress and a corrosive solution [6, 7].

In general, there are two categories of pipeline accidents caused by SCC [8]. One is a high-pH SCC resulting from anodic dissolution (AD) between grain boundaries. The other is a near-neutral pH SCC caused by the combination of AD and hydrogen-induced cracking (HIC). In near-neutral pH solutions, Xu and Cheng found that the effect of static elastic stress on corrosion was not clearly visible because the deposition of corrosion products on the steel surface counteracted the slight increase in corrosion activity [9]. Xu and Cheng reported that a plastic strain caused a more negative corrosion potential of the steel, indicating that the electrochemical activity was enhanced [10]. Mao and Gu believed that under the effect of the local stress field, some hydrogen in the solution diffused into the metal and was enriched around the crack tip [11]. Hydrogen enhanced corrosion of the steel due to hydrogen-induced changes in the corrosion potential and an exchange current density [12]. Fang and Han discovered that a cyclic loading test promoted the transition from corrosion pits to cracks by increasing the local strain rate around the corrosion pits, resulting in SCC of the material [13]. Fan and Liu proposed that metals can form stable and tenacious passive films in higher pH solutions [14]. In addition, the AD rate at the crack tip was reduced by the inhibition of the cathodic reaction, thereby reducing the SCC susceptibility (I_{scc}). Furthermore, Javidi and Horeh asserted that in high pH solutions, the hydrogen-based mechanism dominated the SCC behavior [15].

In practical and complex environments, the SCC mechanism of PH stainless steel is more difficult to understand. Moreover, microbiologically influenced corrosion (MIC) caused by microbial metabolic activities is common in marine and oilfield environments. For example, widely distributed sulfate-reducing bacteria (SRB) can also promote the initiation of SCC cracks [16, 17]. Chen and Wang observed that biofilm formation and sulfide deposition caused the potential difference in a crevice to increase [18]. Domzalicki and Lunarska analyzed the effect of ferrite-pearlite and sorbite microstructures on the hydrogen-assisted cracking of SRB under similar cathodic polarization conditions [19]. The generation of S^{2-} ions and the inhibition of the formation of deposits led to the promotion of hydrogen charging and plasticity loss by the SRB, while the same amount of hydrogen had a decreased detrimental effect on the sorbite steel. However, there is still controversy about the effects of microorganisms on SCC, and it has also been found that microbial activity inhibits corrosion. Gou and Xie found that SRB reduced the I_{scc} of X100 pipeline steel in a slow strain rate tensile test [20]. Gunasekaran and Chongdar reported that microbes can form protective films on the surface of low carbon steel to inhibit corrosion [21]. Therefore, it is necessary to further study the effects of microorganisms on SCC.

Typically, 17-4 PH stainless steel is solution treated at 1020-1060 °C and aged at 480, 550, 580 and 620 °C. Different heat treatment processes produce different microstructures. Most of the previous studies on 17-4 PH stainless steel focused on the effect of the microstructure on the corrosion resistance. When both SRB and applied stress are present, their synergistic effects on the enhanced corrosion of PH stainless steel have not yet been reported. In this paper, 17-4 PH stainless steel samples subjected to three different heat treatments were tested by corrosion exposure. The individual and synergistic effects of the SRB and applied stress typically concurrently encountered in practical applications are systematically examined.

2. EXPERIMENTAL METHODS

2.1 Testing Medium

The sterile test medium in this study was a 3.5 wt.% NaCl solution. The SRB strains used were of the *Desulfovibrio* genus and were cultured in a standard culture medium recommended by the American Petroleum Institute [22]. The sterile solution was deoxygenated by bubbling with pure nitrogen for 0.5 h. The sterile solution and the standard culture medium were incubated at 121°C for 15 min for autoclaving and air cooled to 25 °C. The SRB strain was transferred to a standard culture medium and sealed in an incubator at 30 °C for 5 days. All SRB inoculation procedures were performed in a sterile workstation.

2.2 Materials and Methods

The chemical composition of the 17-4 PH stainless steel samples was as follows (wt.%): C, 0.04; Mn, 0.28; Si, 0.51; S, 0.021; P, 0.027, Cr, 16; Ni, 4.15; Cu, 3.4; and Nb, 0.3. Fig. 1 shows the time and temperature changes for single-stage aging, double-stage aging, and intermediate treatment. These three heat treatment processes are indicated as A, B, and C, respectively. All samples were air cooled to 25 °C. The microstructures of the samples were observed using optical microscopy (OM; Leica DMI5000 M) and transmission electron microscopy (TEM; JOEL JEM-2100F). Scanning electron microscopy (SEM; HITACHI SU8000) was used to characterize the fracture surface morphology of the samples. Energy dispersive spectrometry (EDS) was used to analyze the corrosion products of the samples.

Electrochemical impedance spectroscopy (EIS) was conducted in a PARSTAT2273 electrochemical workstation using a conventional three-electrode electrochemical system. The sinusoidal potential perturbation was 10 mV. The frequency range was 10^5 to 10^{-2} Hz. Axially loaded tensile samples were used to investigate the effects of SRB and applied stress on the corrosion behavior of the PH stainless steel according to ASTM standard G49-85 (reapproved in 2011). The dimensions of the samples are shown in Fig. 2(a), and the device for the SCC experiment is shown in Fig. 2(b). To simulate the stress condition of materials in actual use, the stress frame was fixed after the samples reached 1% strain on the LETRY PLD-20 tensile machine. An insulating material was placed between the samples and the stress frame. The samples and stress frame were sterilized by ultraviolet radiation. The sterile solution and the 5 % inoculated solution (pH 7.5) were prepared according to the actual seawater bacteria content and were transferred to the sealed chamber. The solutions and immersed samples were kept at 25 °C for 21 days. Slow strain rate tensile (SSRT) tests were carried out at a strain rate of 1×10^{-6} s^{-1} on a tensile machine for the immersed samples. In the sterile and SRB-inoculated solutions, three experiments were performed for each heat treatment process to ensure the reliability of the results.

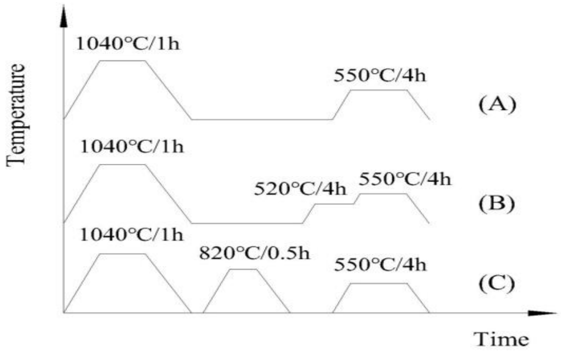

Figure 1. Heat treatment processes (heating rate approximately 150 °C/min and cooling rate approximately 80 °C/min) of 17-4 PH stainless steel: (a) single-stage aging, (b) double-stage aging, and (c) intermediate treatment.

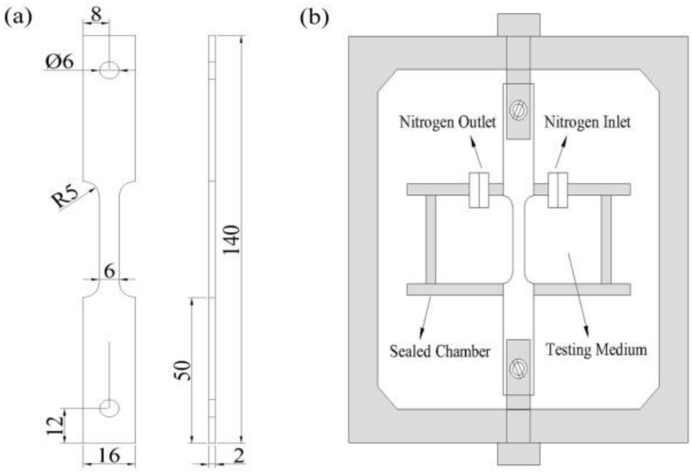

Figure 2. SCC test equipment: (a) dimensions of test specimens (units: mm) and (b) schematic of the test vessel for the SCC experiment.

3. RESULTS

3.1 Microstructures after Different Processes

The microstructures of the 17-4 PH stainless steel are shown in Fig. 3. Obviously, the microstructure was mainly composed of tempered martensite. In addition, it also contained a small amount of ferrite and reverse austenite [23]. Significant heterogeneities, such as coarse martensite and segregation of constituent elements, were observed in the microstructures (Figs. 3(a) and (b)). It can be seen that the tempered martensite increased in size and became evenly distributed in the microstructure after double-stage aging. The amount of tempered martensite and reverse austenite increased, while the amount of ferrite decreased. Fig. 3(c) shows that the size of the martensite was uniform and that the position relationship was distinct.

The TEM images of the microstructures after double-stage aging showed that reverse austenite was formed on the boundary of the lath martensite (Figs. 4 (a) and (b)). The dissolved Cr atoms caused a strong segregation driving force from the intragranular regions to the grain boundaries, which were substantially segregated during the cooling process.

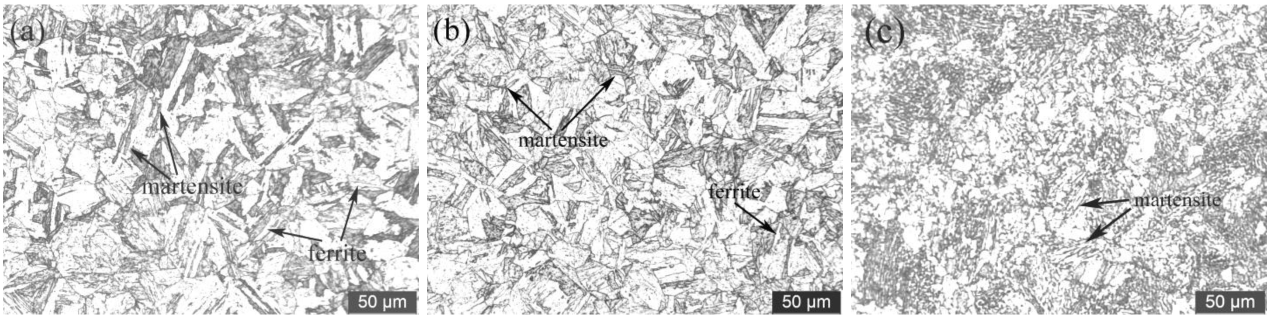

Figure 3. Microstructures of 17-4 PH stainless steel etched by (CuSO4(2 g) + HCl(10 ml) + H2O(10 ml)) solution (observed by OM): (a) single-stage aging, (b) double-stage aging, and (c) intermediate treatment.

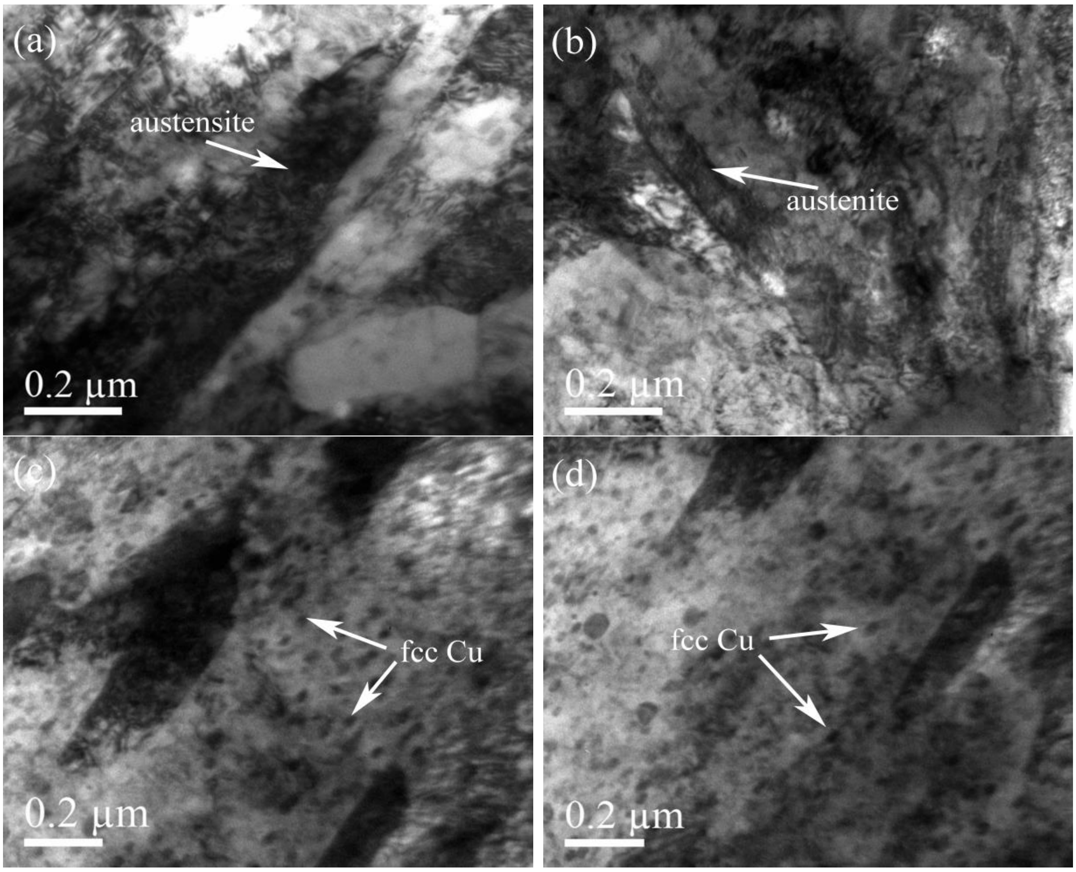

Figure 4. Microstructures of the intragranular precipitates in 17-4 PH stainless steel: (a, b) double-stage aging and (c, d) intermediate treatment.

Such segregation promoted the nucleation of precipitates in crystallites, causing the carbides to precipitate at the grain boundaries and increasing the grain boundary embrittlement, which promoted crack propagation. The TEM images after intermediate treatment showed that the microstructures consisted mainly of tempered martensite and dispersed fcc Cu precipitates in the martensite matrix (Figs. 4(c) and (d)). The small granular fcc Cu precipitates were discretely distributed along grain boundaries and throughout the grains.

3.2 EIS in Different Solutions

The surface characteristics of the 17-4 PH stainless steel samples were inspected by EIS to investigate their corrosion differences. Figure 5 shows the EIS results in different environments. The impedance values of the PH stainless steel were significantly different in the different environments. In summary, the impedance values in the SRB-inoculated environment were smaller than those of the stainless steel in the sterile environment. The stainless steel that received the intermediate treatment in the sterile environment displayed the largest impedance value, while the stainless steel with the double-stage aging had the smallest impedance value. Therefore, the corrosion resistance behavior was improved by the intermediate treatment. The value of the phase angle increased as the frequency in the low frequency range increased. However, the phase angle in the SRB-inoculated solution was greater than that of the sterile solution, indicating the presence of a film layer in the SRB-inoculated solution [24].

The equivalent circuit R (C(R(CR))), shown in Fig. 6, was used for fitting the EIS spectra. The impedance value of the 17-4 PH stainless steel at high frequencies in the SRB-inoculated solution was lower than the impedance value in the sterile solution. The high-frequency resistance is related to the R_e value [25], which indicated an increase in the conductivity of the SRB-inoculated solution. The low-frequency resistance is related to R_c and R_{ct}. Table 1 shows the electrochemical impedance fitted values in the SRB inoculating solution. In the SRB-inoculated solution, the elevated resistance value indicates greater resistance to changes in the surface structure of the electrode, thus implying better corrosion resistance behavior.

Table 1. Electrochemical impedance fitted values in SRB-inoculated solution

Process	R_c (Ω·cm^2)	R_{ct} (Ω·cm^2)
single-stage aging	390.2	5762
double-stage aging	187.4	1074
intermediate treatment	533.7	9456

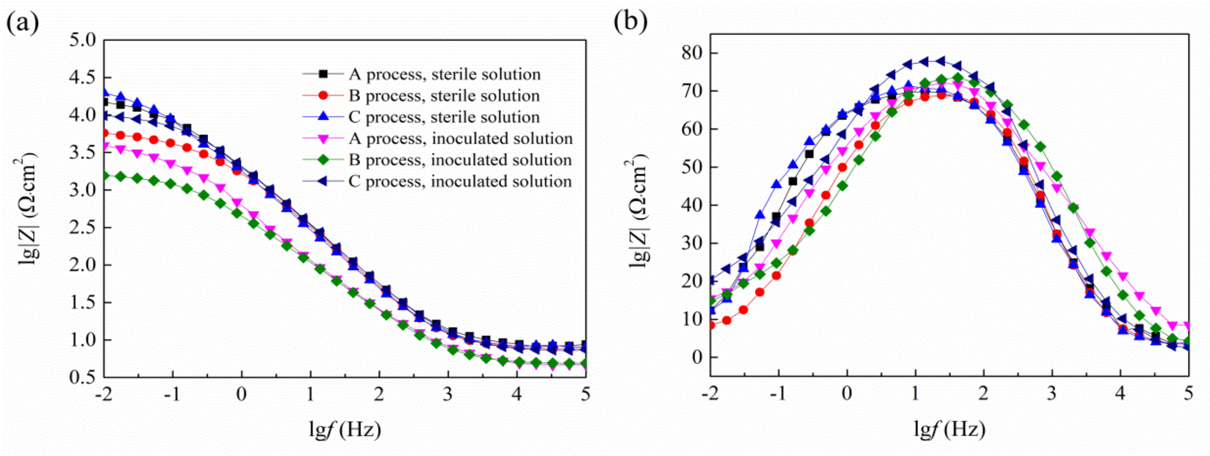

Figure 5. Bode plots of 17-4 PH stainless steel after different aging treatment: (a) Bode |Z| diagram, and (b) Bode phase diagram.

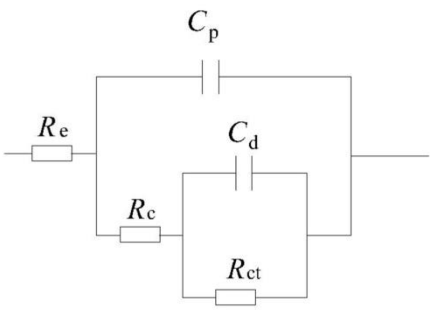

Figure 6. Equivalent circuit diagram of 17-4 PH stainless steel: R_e is the electrolyte resistance, C_p is the pure capacitance, C_d is the double-layer capacitance, R_c is the corrosion product resistance, and R_{ct} is the charge transfer resistance.

3.3 Mechanical Properties after exposure to SRB

The stress–strain curves of 17-4 PH stainless steel in sterile and inoculated solutions are displayed in Fig. 7(a). The 17-4 PH stainless steel in the SRB-inoculated solution exhibited a similar stress–strain relationship as that tested in the sterile solution. However, the yield strength under sterile conditions was higher than that in the inoculation conditions. In the sterile solution, the yield strength after the double-stage aging process was higher than that after the single-stage aging process, and the values were approximately 1010 and 980 MPa, respectively. However, in the SRB-inoculated solution, the yield strength of the double-stage aging process was lower than that after the single-stage aging process, and the values were approximately 950 and 970 MPa, respectively. This result indicated that the double-stage aging of 17-4 PH stainless steel was the most sensitive to the SRB. The steel that underwent the intermediate treatment consistently expressed the lowest yield strength and the largest fracture strain among the three conditions. The reduction of area (ψ) is displayed in Fig. 7(b). Compared with the sterile solution, the reduction of area after single-stage aging, double-stage aging and intermediate treatment in the SRB-inoculated solution approximately decreased by 5.38, 7.74 and

3.72%, respectively. This result further confirmed that the double-stage aged samples were most sensitive to SRB among the three conditions.

Figure 8 shows the microscopic fracture surface morphology after SSRT testing of the 17-4 PH stainless steel in the sterile and inoculated solutions. Large and irregular-shaped dimples and microvoids were detected on the fracture surface of the intermediate treated sample tested in the sterile solution (Fig. 8(c)), which expressed the typical ductile fracture characteristics of 17-4 PH stainless steel. Similar fracture morphology characteristics were observed on the sample tested in SRB-inoculated solution (Fig. 8(f)). Some microvoids were connected by microcracks, which were not found on the fracture surface in the sterile solution. This morphology still belongs to the ductile fracture category. The substantial drop in toughness of the single-stage aged samples was also visible in the fracture morphology shown in Figs. 8(a) and (d). In the sterile solution, cleavage cracks formed along parallel cleavage planes of different heights, and the cracks converged to form a step on the surface of the crack. In the SRB-inoculated solution, narrow and long cracks were discovered on the fracture surface.

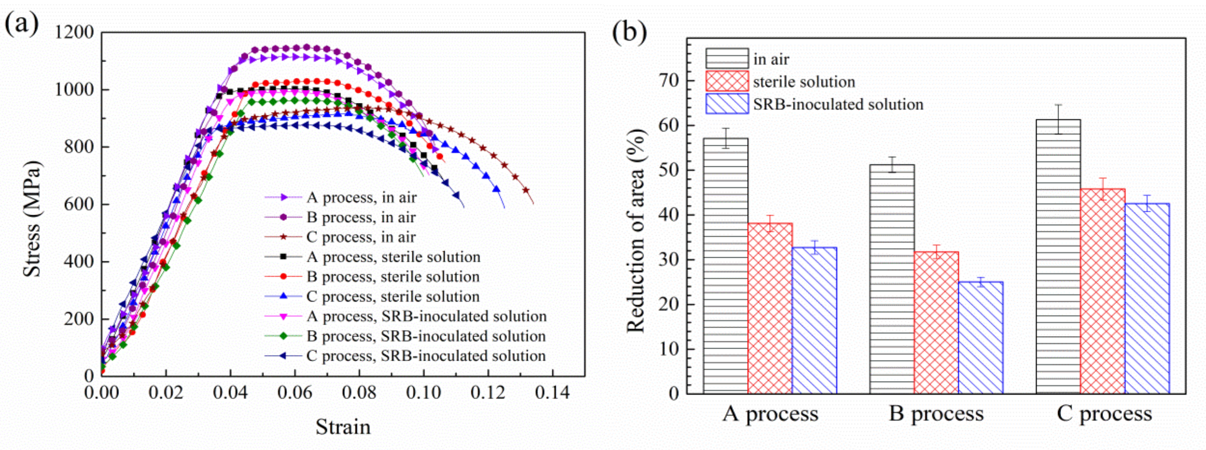

Figure 7. Stress-strain curve of materials subjected to three different heat treatment processes in different media: (a) stress-strain curves and (b) reduction of area.

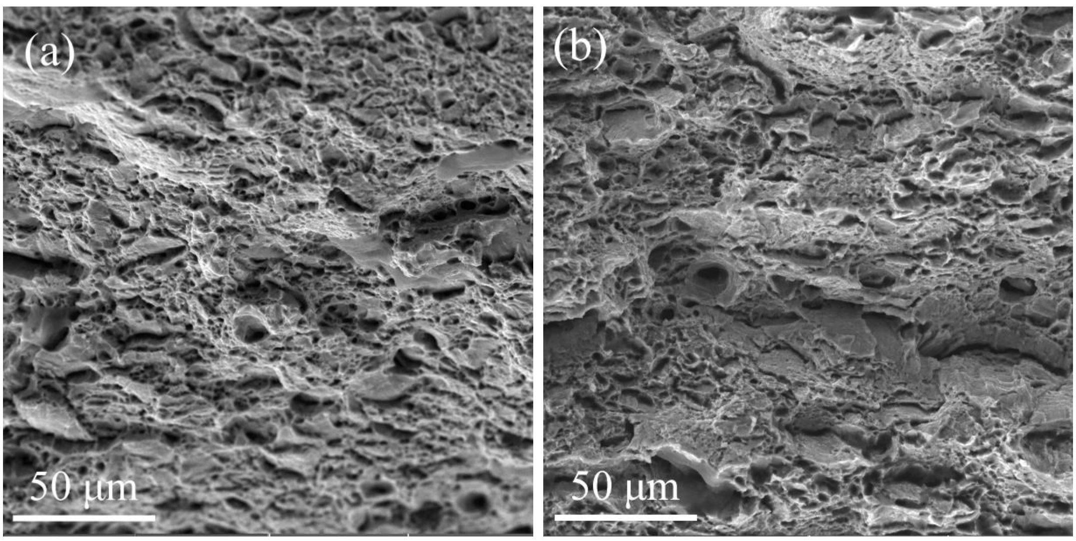

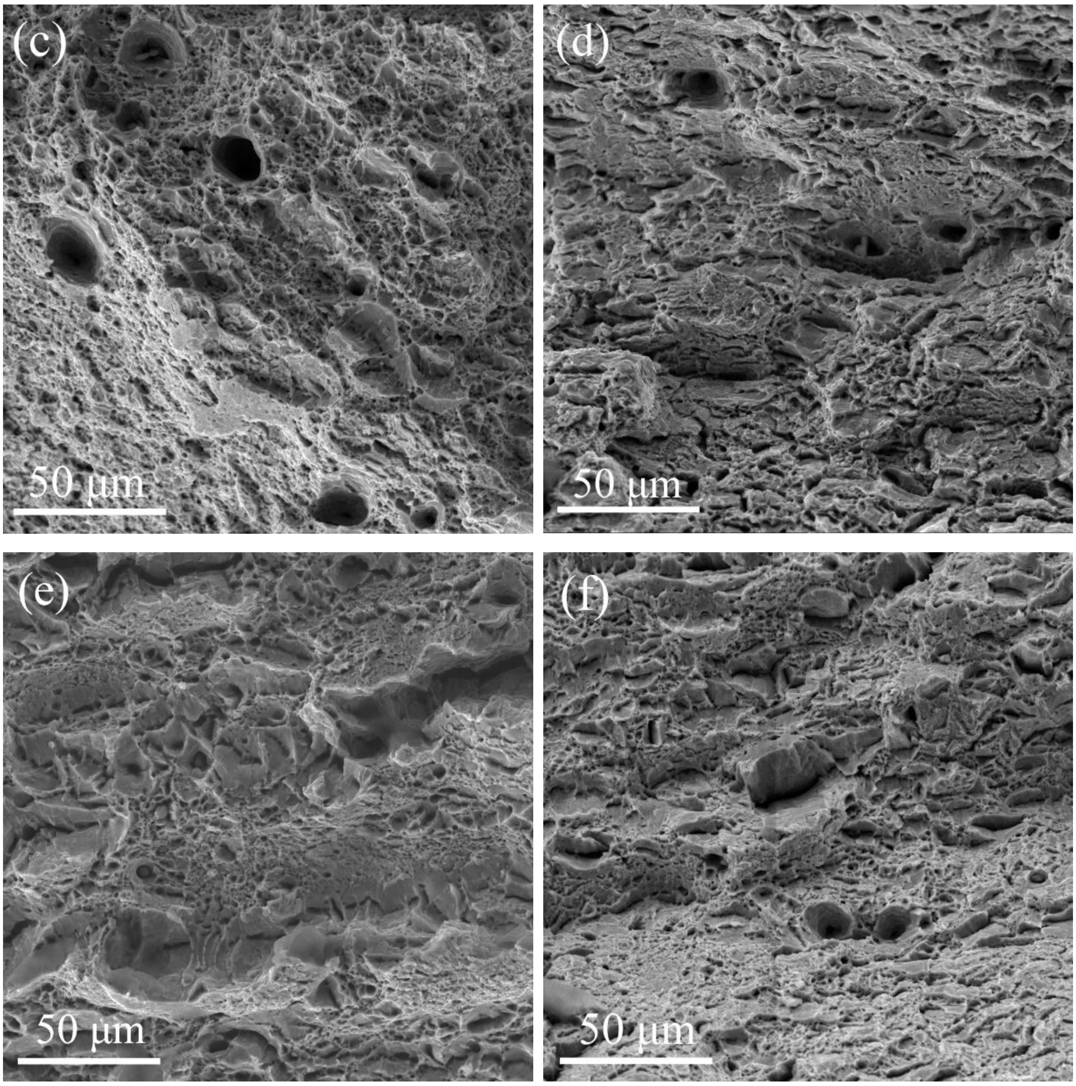

Figure 8. Fracture morphologies of 17-4 PH stainless steel: (a) A process, sterile solution; (b) B process, sterile solution; (c) C process, sterile solution; (d) A process, SRB-inoculated solution; (e) B process, SRB-inoculated solution; and (f) C process, SRB-inoculated solution.

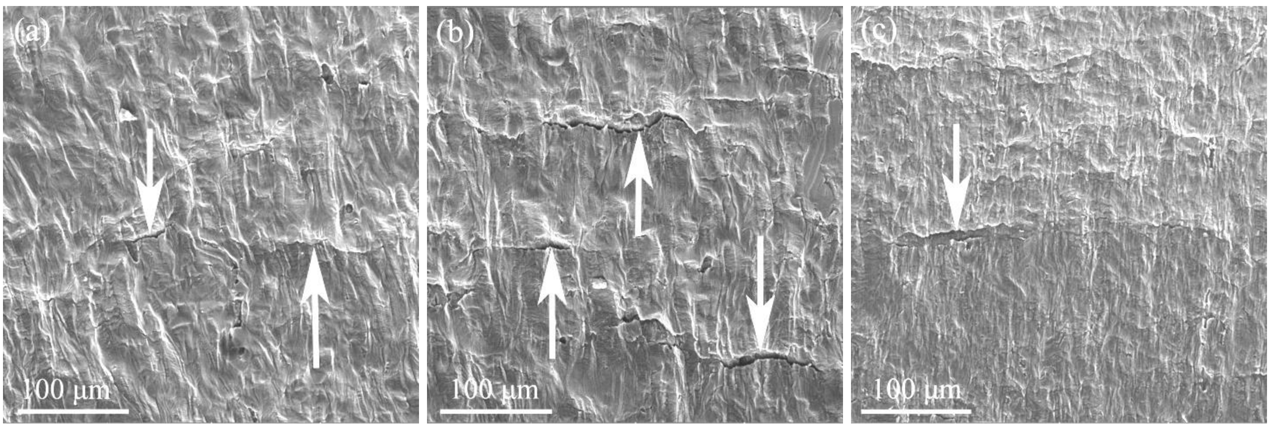

Figure 9. The lateral fracture morphologies of 17-4 PH stainless steel in SRB-inoculated solution: (a) single-stage aging, (b) double-stage aging, and (c) intermediate treatment.

In the double-stage aged samples, deep and wide cracks were observed (Figs. 8(b) and (e)). A large crack corresponds to deterioration in the reduction of area. This confirms that the double-stage aged 17-4 PH stainless steel was most sensitive to SRB among the three conditions.

The micrographs of the lateral surface morphology after SSRT testing of the 17-4 PH stainless steel in the SRB-inoculated solution are shown in Fig. 9. For all samples, the captured area was approximately 300 µm from the fracture line. The lateral surface micrographs under different heat treatment conditions showed different morphological features. Some bent and narrow microcracks occurred on the lateral surfaces of the sample that underwent single-stage aging (Fig. 9(a)). A similar morphology was observed for the sample that underwent intermediate treatment (Fig. 9(c)). However, the cracks that appeared on the double-stage aged sample were straight and deep (Fig. 9(b)), which is consistent with the decreased reduction of area and sensitivity to the SRB.

3.4 Corrosion Morphology and EDS after SRB

Fig. 10 shows the corrosion morphology and EDS of the 17-4 PH stainless steel in the SRB-inoculated solution. The single-stage aged sample showed a long strip-shaped corrosion zone (Fig. 10(a)). The lath martensite was obvious in the microstructure of the sample with single-stage aged treatment. Under the synergistic effects of a stress and the SRB, the lath martensite promoted crack initiation, and the corrosion at the crack was intensified, forming a corrosion zone.

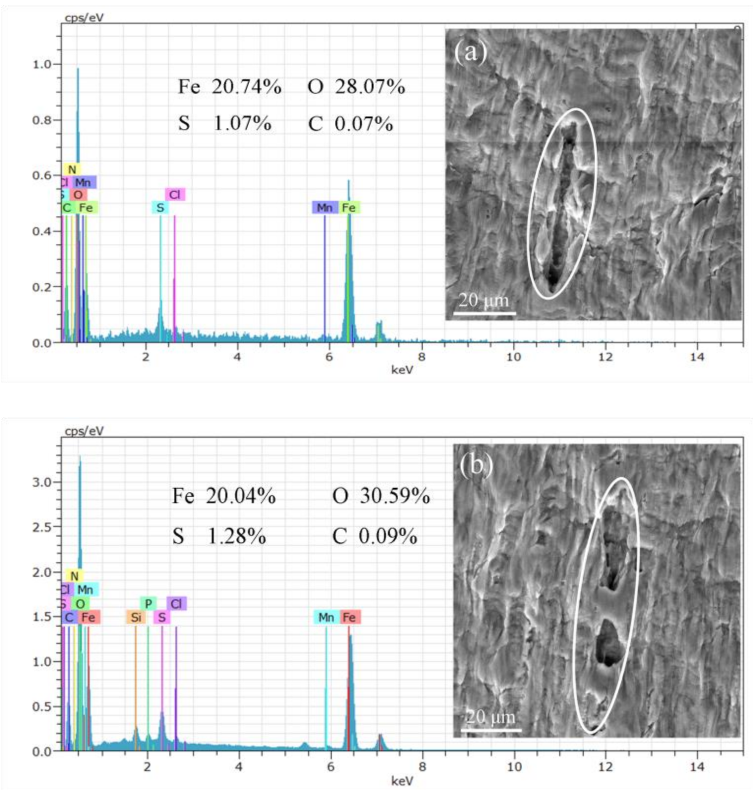

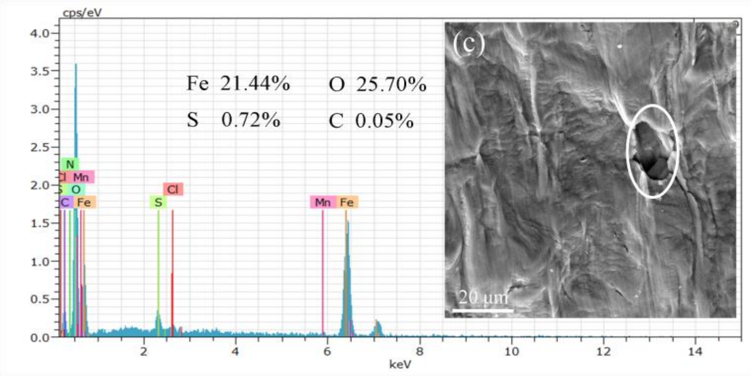

Figure 10. The corrosion morphologies and EDS of the 17-4 PH stainless steel in the SRB-inoculated solution: (a) single-stage aging, (b) double-stage aging, and (c) intermediate treatment.

The double-stage aged sample exhibited the coexistence characteristics of a corrosion pit and a long strip-shaped corrosion zone (Fig. 10(b)). Compared with the single-stage aged sample, the corrosion zone was wide and the corrosion pit was obvious. A large amount of coarse tempered martensite in the microstructures of the double-stage aged sample contributed to crack propagation. The content of S was higher, and the synergistic effects were obvious. A corrosion pit appeared on the surface of the intermediate-treatment sample, but no corrosion zone was found (Fig. 10 (c)). The uniform and fine martensite of the intermediate treatment sample hindered the crack initiation. A lower amount of S means that the corrosion reaction rate was decreased and the synergistic effects were not significant.

4. DISCUSSION

Wu and Xu proposed a comprehensive evaluation index consisting of steel/solution component properties, SRB activity, applied stress, and their simultaneous effects [26]. However, evaluation criteria based on corrosion processes cannot be well adapted to the evaluation of I_{scc} because I_{scc} evaluation indexes include elongation and reduction of area. However, there is hydrogen in the SRB-inoculated solution, and hydrogen-induced local plasticity has been reported previously [27-29], which may lead to an abnormal elongation of samples. Therefore, the I_{scc} was measured by the reduction of area. The I_{scc} was derived by Eq. (1) and Eq. (2) [30]:

$$\psi = (A_0 - A_1)/A_0 \times 100\%, \quad (1)$$

where A_0 is the original cross-sectional area of the specimen (mm^2) and A_1 is the cross-sectional area of the specimen after fracture (mm^2).

$$I_{scc} = (1 - \psi_s/\psi_a) \times 100\%, \quad (2)$$

where ψ_s is the reduction of area tested in sterile and SRB-inoculated solutions, and ψ_a is the reduction of area tested in air. The larger the value of I_{scc}, the more susceptible the material is to SCC. Table 2 shows the I_{scc} values of the 17-4 PH stainless steel in sterile and SRB-inoculated solutions. It can be seen that SRB improved the SCC susceptibility of the samples regardless of the heat treatment process. The changes in the I_{scc} of the single-stage aging, double-stage aging and intermediate-treatment samples were 5.2, 9.3 and 4.4%, respectively. That is, in the SRB-inoculated solution, the double-stage aging samples were the most susceptible to SCC among the tested samples.

4.1 Individual Role of Applied Stress

It is generally believed that localized corrosion, such as the formation of corrosion pits, is a key precursor of microcrack nucleation [31, 32]. Under an applied stress, the electrochemical activity at a crack tip is enhanced, which is also known as the mechanochemical effect [33]. The samples prepared by double-stage aging contained a large amount of tempered martensite, which produced the largest yield strength among the samples herein but also promoted crack initiation. Meanwhile, the interaction between the carbides and the martensite matrix provided a potential source of cracking [34]. Once the microcracks were initiated, the crack tip acted as the anode and the crack wall acted as the cathode. Electrochemical corrosion between the crack wall and the crack tip promoted crack propagation. Therefore, the double-stage aged samples showed the largest I_{scc} value among the samples herein. For the intermediate-treatment samples, the formation of fine precipitates by Cu precipitation and the martensite matrix interaction strengthened the material, and the fine uniform martensitic not only improved the toughness of the stainless steel but also impeded crack initiation. Under the applied stress, the inclusions and the matrix metal formed activation zones within the metal. Once the material exhibited localized corrosion due to the synergistic effects of stress concentration and corrosive solution, localized corrosion sites initiated cracks [35-37].

4.2 Individual Role of SRB

In the alternative theory, the MIC mechanism of SRB, the explanation of MIC is not directly related to the bacteria itself [38]. Generally, microorganisms located on, or adjacent to, the metal do not directly attack the metal. They induce or promote corrosion through by-products of metabolism [39]. In the SRB-inoculated solution, the electrode reactions were as follows:

$$\mathrm{Fe} \rightarrow \mathrm{Fe}^{2+} + 2\mathrm{e}^{-} \tag{3}$$

$$\mathrm{SO_4^{2-}} + 8\mathrm{H} \xrightarrow{\mathrm{SRB}} \mathrm{S}^{2-} + 4\mathrm{H_2O} \tag{4}$$

$$\mathrm{H_2O} \rightarrow \mathrm{H}^{+} + \mathrm{OH}^{-} \tag{5}$$

$$\mathrm{Fe}^{2+} + \mathrm{S}^{2-} \rightarrow \mathrm{FeS} \tag{6}$$

$$2\mathrm{H}^{+} + \mathrm{S}^{2-} \rightarrow \mathrm{H_2S}\,. \tag{7}$$

Partial S^{2-} and Fe^{2+} generated by the AD mutually adsorbed, deposited, and detached from the electrode surface, which consequently enhanced the AD process and accelerated the corrosion reaction [40]. In addition, Fe-containing sulfide is highly conductive [41], increasing the solution conductivity. Some of the S^{2-} and H^{+} in solution were combined to generate H_2S, which completed the sulfate reduction process. H_2S itself is a catalyst for hydrogen permeation, which can effectively accelerate the penetration of hydrogen into the interior of the metal; however, hydrogen permeation reduced the cohesive energy and toughness of the material [42]. The formation of the aggressive corrosive metabolite H_2S promoted the rate of metal corrosion [43]. However, the ability of H^+ to attract electrons is weaker than that of Fe^{2+}, so the generation of FeS was dominant.

4.3 The Synergistic Effects of Applied Stress and SRB

In the SRB-inoculated solution, the applied stress and SRB played important roles in the corrosion process. The applied stress caused an increase in the porosity of the corrosion film on the surface of the material. Once the corrosive solution was in direct contact with the material through the film, the film did not provide protection against corrosion of the steel. The bottom of the film corresponded to the tip of the crack, which accelerated the corrosion under stress. The applied stress may cause plastic deformation of the crack tip. The mechanochemical effect produced by plastic strain became significant, and the AD rate of the steel increased rapidly [44, 45]. For the single-stage aging and intermediate process samples, the EIS showed high impedance values and improved surface film integrity. These samples had an increased reduction of area, and the fracture surface dimples and microcracks coexisted, and there were no obvious secondary cracks on the lateral surfaces. It is reasonable to assume that the fracture mechanism was AD. For the double-stage aged sample, the dislocations and the coarse lath martensite provided an enrichment region for the production of hydrogen from the cathode reaction. EIS showed the lowest impedance values for double-stage aged sample compared to that of the other samples and poor surface film integrity; also, the reduction of area was also the lowest, and the I_{scc} had the maximum value. The fracture morphology exhibited a wide crack, and the lateral surface presented a sharp and narrow single crack. Based on these observations, the fracture mechanism for double-stage aged sample was HIC.

SRB can scavenge cathodic hydrogen and electrons from steel to reduce sulfate to sulfide [46]. In addition, the ruptured film can also entrap deleterious metabolites secreted by the SRB, such as FeS, which reduces the corrosion resistance of stainless steel by creating pitting corrosion on the surface [47, 48]. However, in the SRB-inoculated solution, the bacterial metabolism disrupted the stability of the sulfide films. The active corrosion cell between the FeS film (cathode) and the metal substrate (anode) significantly accelerated the corrosion rate [49]. The characteristics of the steel surface were altered by this ruptured film. Once microcracks occurred, the corrosion activity of the stainless steel increased rapidly.

Therefore, it is reasonable to believe that SRB and an applied stress alter the properties of the interface between the steel and the solution, and harmful metabolites secreted by the SRB, such as FeS and H_2S, enhanced the corrosion of the 17-4 PH stainless steel.

Table 2. I_{scc} values of samples after different heat treatments in sterile and SRB-inoculated solutions ($\bar{I}_{scc}$ represents average values)

Process	I_{scc} (sterile solution) (%)			I_{scc} (SRB-inoculated solution) (%)			$\bar{I}_{scc}$(SRB-inoculated solution) - $\bar{I}_{scc}$(sterile solution) (%)
A process	34.8	36.7	38.1	39.7	42.2	43.2	5.2
B process	39.4	42.3	43.6	47.2	52.8	53.1	9.3
C process	22.3	25.8	26.7	27.2	30.2	30.7	4.4

5. CONCLUSIONS

(1) The microstructure of single-stage aged and double-stage aged samples mainly consisted of ferrite and coarse tempered martensite. The microstructure of the martensite in the samples that underwent intermediate treatment was more uniform than that of the other samples considered herein and the position relationship was distinct.

(2) Under the individual effect of applied stress, the large size of tempered martensite in the double-stage aged sample promoted crack initiation, resulting in the highest yield strength and I_{scc} value among the samples considered herein.

(3) In the SRB-inoculated solution, the production of FeS and H_2S enhanced the AD process and hydrogen permeation, accelerating the corrosion reaction. Compared with the sterile solution, the impedance value decreased and I_{scc} increased.

(4) Under the synergistic effects of the applied stress and SRB, the SCC mechanism for single-stage aged and intermediate treated samples was AD, and that for the double-stage aged samples was HIC.

ACKNOWLEDGEMENTS
This work was supported by the National Natural Science Foundation of China (Grant number 51574147), the Natural Science Foundation of Liaoning Province (Grant number 201602474) and the 'GDAS' Project of Science and Technology Development (2019GDASYL-0203002).

References

1. S. Pahlavan, S. Moazen, I. Taji, K. Saffar, M. Hamrah, M.H. Moayed and S. Mollazadeh Beidokhti, *Corros. Sci.*, 112 (2016) 233.
2. J. Wang, H. Zou, C. Li, S.Y. Qiu and B.L. Shen, *Charact.*, 59 (2008) 587.
3. H. Riazi, F. Ashrafizadeh, S.R. Hosseini and R. Ghomashchi, *Mater. Sci. Eng. A*, 703 (2017) 262.
4. M. Esfandiari and H. Dong, *Surf. Eng.*, 22 (2016) 86.
5. S.V. Raj, L.J. Ghosn, B.A. Lerch, M. Hebsur, L.M. Cosgriff and J. Fedor, *Mater. Sci. Eng. A*, 456 (2007) 305
6. B.M. Schönbauer, K. Yanase and M. Endo, *Theor. Appl. Fract. Mech.*, 87 (2017) 35.
7. Q.L. Zhang, Z.Q. Hu, W.W. Su, H.L. Zhou, C.X. Liu, Y.L. Yang and X.W Qi, *Surf. Coat. Technol.*, 321 (2017) 64.
8. F.L. Sun, S. Ren, Z. Li, Z.Y. Liu, X.G. Li and C.W. Du, *Mater. Sci. Eng. A*, 685 (2017) 145.
9. L. Y. Xu and Y. F. Cheng, *Corros. Sci.*, 59 (2012) 103.
10. L. Y. Xu and Y. F. Cheng, *Corros. Sci.*, 64 (2012) 145.
11. S.X. Mao, B. Gu, N.Q. Wu and L. Qiao, *Philos. Mag. A.*, 81 (2001), 1813.
12. M. C. Li and Y. Cheng, *Electrochim. Acta.*, 52 (2007) 8111.
13. B.Y. Fang, E.H. Han, J.Q. Wang and W. Ke, *Corros. Eng., Sci. Technol.*, 42 (2007) 123.
14. L. Fan, Z.Y. Liu, W.M. Guo, J. Hou, C.W. Du and X.G. Li, *Acta Metall. Sin.*, 28 (2015) 866.
15. M. Javidi and S. Bahalaou Horeh, *Corros. Sci.,* 80 (2014) 213.
16. S. Sh. Abedi, A. Abdolmaleki and N. Adibi, *Eng. Fail. Anal.*, 14 (2007) 250.
17. D. X. Sun, M. Wu and F. Xie, *Mater. Sci. Eng. A*, 721 (2018) 135.
18. X. Chen, G.F. Wang, F.J. Gao, Y.L. Wang and C. He, *Corros. Sci.*, 101 (2015) 1.
19. P. Domżalicki， E. Lunarska and J. Birn, *Mater. Corros.,* 58 (2007) 413.
20. W. Gou, B. Xie, Chong Xu. Z. Zheng. J. He. D. Huang and N. Geng, *Int. J. Electrochem. Sci.,* 14

(2019) 494.
21. G. Gunasekaran, S. Chongdar, S. Gaonkar and P. Kumar, *Corros. Sci.*, 46 (2004) 1953.
22. S. Païssé, J.F. Ghiglione, F. Marty, B. Abbas, H. Gueuné , J.M.S. Amaya, G. Muyzer and L. Quillet, Appl. Microbiol. Biotechnol., (97) 2013 7493.
23. Y.X. Wu, R.M. German, D. Blaine, B. Marx and C. Schlaefer, *J. Mater. Sci.*, 37 (2002) 3573.
24. M.C. Yan, J. Xu, L. Yu, T.Q. Wu, C. Sun and Ke, W, *Corros. Sci.*, 110 (2016) 23.
25. L. Hao, S. Zhang, J. Dong and W. Ke, *Corros. Sci.*, 58 (2012) 175.
26. T.Q. Wu, J. Xu, M.C. Yan, C. Sun, C.K. Yu and W. Ke, *Corros. Sci.*, 83 (2014) 38.
27. D. Delafosse and T. Magnin, *Eng. Fract. Mech.*, 2001, vol. 68 (2001) 693.
28. X.C. Ren, W.Y. Chu, Y.J. Su, J.X. Li, L.J. Qiao, B. Jiang, M.R. Zhang and G. Chen, *Mater. Sci. Eng. A*, 491 (2008) 164.
29. H.C. Ma, Z.Y. Liu, C.W. Du, H.R. Wang, C.Y. Li and X.G. Li, *Mater. Sci. Eng. A*, 642 (2015) 22.
30. A. Torres-Islas and J. G. González-Rodríguez, *Int. J. Electrochem. Sci.*, 4 (2009) 640.
31. F. Xie, D. Wang, M. Wu, C.X. Yu, D.X. Sun, X. Yang and C.H. Xu, *Metall. Mater. Trans. A*, 49 (2018) 1372.
32. P.K. Singh Raman, *Sadhana*, 28 (2003) 467.
33. T. P. Hoar and J. M. West, *Proc. R. Soc. Lond.*, 268 (1962) 304.
34. Y. Luo, J.M. Pang, H.B. Wang and X.C. Wu, *Mater. Sci. Eng. A*, 527 (2010) 3433.
35. Ibrahim M. Gadala and Akram Alfantazi, *Metall. Mater. Trans. A*, 46 (2015) 3104.
36. S. L. Asher and P. M. Singh, *Corrosion*, 65 (2009) 79.
37. P. Liang, X.G. Li, C.W. Du and X. Chen, *Mater. Des.*, 30 (2009) 1712.
38. X. Wang, Z. Peng, S. Zhong, G. Wang, Q. Hu and Y. Li, *Int. J. Electrochem. Sci.*, 13 (2018) 8970.
39. K. Y. Chan, L.C. Xu and H. P. Fang, *Environ. Sci. Technol.*, 36 (2002) 1720.
40. D. Wang, F. Xie, M. Wu, G.X. Liu, Y. Zong and X. Li, *Metall. Mater. Trans. A*, 48 (2017) 2999.
41. Homero Castaneda and Xochitl D. Benetton, *Corros. Sci.*, 50 (2008) 1169.
42. K.M. Usher, A.H. Kaksonen, I. Cole and D. Marney, *Int. Biodeterior. Biodegrad.*, 93 (2014) 84.
43. R. Jia, J. L. Tan and P. Jin, *Corros. Sci.*, 130 (2018) 1.
44. B.T. Lu, J.L. Luo, P.R. Norton and H.Y. Ma, *Acta Mater.*, 57 (2009) 41.
45. J.Q. Wang, J. Chen, E.H. Han and W. Ke, *Mater. Trans.*, 49 (2008) 1052.
46. J,Z, Duan, S.R. Wu, X.J. Zhang, G.Q. Huang, M. Du and B.R. Hou, *Electrochim. Acta*, 54 (2008) 22.
47. Kh. MIsmail, A. Jayaraman, T.K. Wood and J.C. Earthman, *Electrochim. Acta*, 44 (1999) 4685.
48. X. X. Sheng, Y. P. Ting and Simo Olavi Pehkonen, *Corros. Sci.*, 49 (2007) 2159.
49. M. Y. Lv and M. Du, *Rev Environ Sci Biotechnol*, 17 (2018) 431.